Chemistry & Biology, Vol. 10, 989–995, October, 2003, ©2003 Elsevier Science Ltd. All rights reserved. DOI 10.1016/j.chembiol.2003.09.015

Enzyme-Assisted Suicide: Molecular Basis for the Antifungal Activity of 5-Hydroxy-4-Oxonorvaline by Potent Inhibition of Homoserine Dehydrogenase

Suzanne L. Jacques,[1,7] I. Ahmad Mirza,[2,7] Linda Ejim,[1] Kalinka Koteva,[1] Donald W. Hughes,[3] Kirk Green,[3] Robert Kinach,[4] John F. Honek,[4] Hoi Kiong Lai,[5] Albert M. Berghuis,[2,6] and Gerard D. Wright[1,*]

[1]Antimicrobial Research Centre and Department of Biochemistry
McMaster University
Hamilton L8N 3Z5
[2]Department of Biochemistry
McGill University
Montreal H3G 1Y6
[3]Department of Chemistry
McMaster University
Hamilton L8S 4M1
[4]Department of Chemistry
University of Waterloo
Waterloo N2L 3G1
[5]Crompton Corporation
Guelph N1E 5L7
[6]Department of Microbiology and Immunology
McGill University
Montreal H3A 2B4
Canada

Summary

The structure of the antifungal drug 5-hydroxy-4-oxonorvaline (HON) in complex with its target homoserine dehydrogenase (HSD) has been determined by X-ray diffraction to 2.6 Å resolution. HON shows potent in vitro and in vivo activity against various fungal pathogens despite its weak (2 mM) affinity for HSD in the steady state. The structure together with structure-activity relationship studies, mass spectrometry experiments, and spectroscopic data reveals that the molecular mechanism of antifungal action conferred by HON involves enzyme-dependent formation of a covalent adduct between C4 of the nicotinamide ring of NAD^+ and C5 of HON. Furthermore, novel interactions are involved in stabilizing the (HON•NAD)-adduct, which are not observed in the enzyme's ternary complex structure. These findings clarify the apparent paradox of the potent antifungal actions of HON given its weak steady-state inhibition characteristics.

Introduction

The increasing frequency of disease resulting from pathogenic fungi has become a serious health concern [1, 2]. The rise in fungal infections is predominantly attributable to an increase in immunocompromised individuals, who are especially susceptible to fungal pathogens, and to failure of present antifungal therapies due to drug resistance [3, 4]. Consequently, the discovery of new antifungal agents and the identification of appropriate targets are pressing. One promising antifungal compound is 5-hydroxy-4-oxonorvaline [HON; (*S*)-2-amino-4-oxo-5-hydropentanoic acid; RI-331], which was isolated from *Streptomyces* species over 40 years ago in an antimycobacterial screen [5] (Figure 1A). HON has been shown to have in vitro effects against the human fungal pathogen *Cryptococcus neoformans* [6] and the plant pathogen *Cladosporium fulvus* [7]. Furthermore, in vivo efficacy against the human pathogen *Candida albicans* has also been shown. Treatment of mice with systemic candidiasis increased survival rates dramatically (100% with 100 mg/kg twice daily over 14 days) while demonstrating no toxicity ($LC_{50} > 5000$ mg/kg) [6].

Early reports identified the target of HON to be homoserine dehydrogenase (HSD) [8], which catalyzes the conversion of *L*-aspartate β-semialdehyde (ASA) to *L*-homoserine (Hse; Figure 1B). HSD is part of the aspartate pathway that synthesizes the essential amino acids methionine, threonine, and isoleucine in fungi. This pathway is absent in mammals making it an excellent target for novel antifungal agents. The effect of HON for treatment of systemic mycoses is remarkable given the unimpressive reversible inhibition characteristics of HSD in the steady state with mM affinity in the metabolically forward, Hse-forming direction (*Ki* of 2 mM) [9]. This tepid affinity of antibiotic for the target would appear to be inconsistent with a compound capable of arresting cell growth. The observation that the affinity was improved in the reverse, i.e., Hse-oxidizing direction, and that this inhibition was potentiated by the presence of the cosubstrate $NADP^+$ [9], suggested a more complex mechanism of inhibition than simple dissociation. Using a combination of structure activity relationships, spectroscopic studies, and X-ray crystallography, we have established the mechanism of HSD inhibition by HON, and consequently the molecular basis for its antifungal properties.

Results and Discussion

Kinetics and Chemical Prerequisites of HSD Inhibition by HON

We established that HSD inhibition by HON exhibited the characteristics of irreversible inactivation rather than a dissociable inhibitor, including both time and concentration-dependent inactivation of HSD (Figure 2), and that inactivation required the presence of $NAD(P)^+$. Inhibition of HSD by HON decreased with increasing ASA concentrations consistent with active site-directed inactivation and preincubation of the inhibitor and NAD^+ did not affect inactivation rates. Two additional HON analogs, isosteric *L*-aspartate β-hydroxamate (a reversible inhibitor of yeast HSD [10]) and 4-oxo-*L*-norvaline (Figure 1A), were also investigated and showed no time-dependent inactivation of HSD. This structure activity analysis suggests that HON-dependent inactivation of

*Correspondence: wrightge@mcmaster.ca
[7]These authors contributed equally to this work.

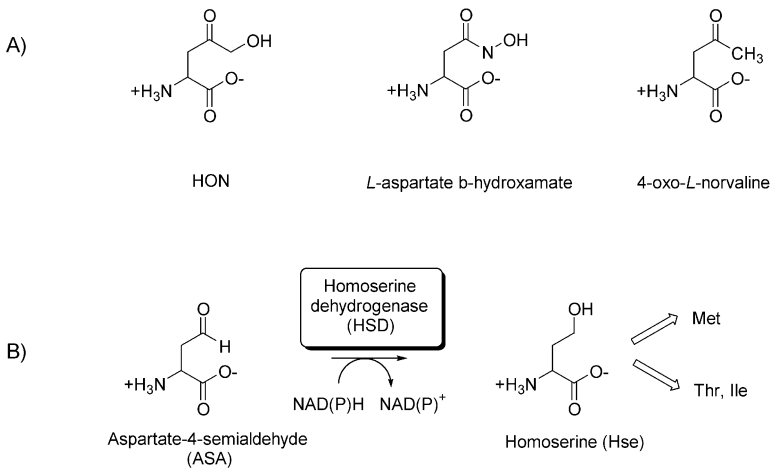

Figure 1. HSD Reaction and Inhibitors

(A) Chemical structures for HON and two analogs thereof.

(B) Reaction catalyzed by HSD.

HSD requires the hydroxymethylketone moiety. Furthermore, 3-amino-pyridine adenosine dinucleotide, a nonreactive NAD^+ analog and competitive inhibitor of nicotinamide cosubstrate binding to HSD [11, 12], was incubated with HSD and HON, and no inactivation of HSD was observed. A redox-active form of $NAD(P)^+$ is therefore essential for inactivation and could be involved in the conversion of HON to an inhibitory form.

Stability of the HSD•NAD(P)$^+$•HON Complex

The reversibility of HON inactivation of yeast HSD was examined by measuring the reappearance of HSD activity and by exchange of [^{14}C]-NAD^+ into an inactive complex; however, no regain of activity or label exchange could be detected after room temperature incubation over 28 days. Inactivation of HSD with HON in the presence of [^{14}C]-labeled NAD^+ resulted in an observed stoichiometry of 1 mol [^{14}C]-NAD^+:1 mol HSD at 100% enzyme inactivation. Electrospray mass spectrometry performed under slightly acidic conditions (0.005% formic acid) revealed a molecular mass of 78,333 ± 100, corresponding to two HON molecules and two NAD^+ molecules bound to the HSD dimer (predicted mass: 78,384). In the absence of HON, or under harsher, protein-denaturing, acidic or basic conditions, only the monomeric species was detected (38,375 ± 10). These results indicate that HON inactivation is a consequence of the formation of a long-lived HSD•NAD^+•HON ternary complex that is sensitive to acid and base denaturation.

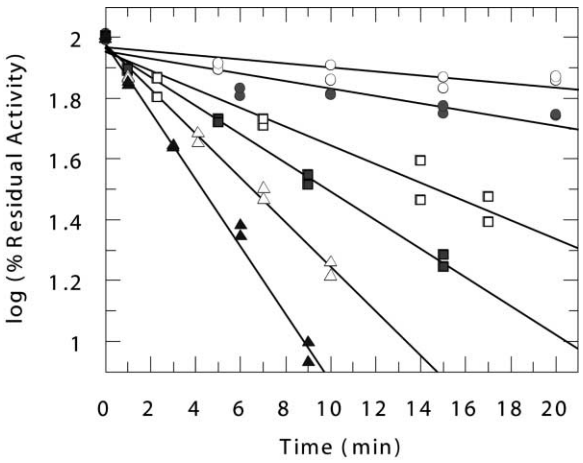

Figure 2. Time-Dependent Inactivation of Yeast HSD by HON

Residual HSD activity was measured at specific times after HSD (0.12 μM) incubation with 0 (○), 0.12 (●), 0.6 (□), 1.2 (■), 2.4 (Δ), and 4.8 mM (▲) HON in the presence of 0.5 mM NAD^+ and 100 mM HEPES (pH 7.5) at room temperature (25°C). Lines represent the results of linear regressions. A plot of first order inactivation rate constants (k_{obs}) versus HON concentration data resulted in a hyperbolic curve and estimation of the maximal rate of inactivation (k_{inact}) of 0.20 ± 0.03 min^{-1} and dissociation constant of K_I = 3.3 ± 0.9.

Inhibition of HSD through Adduct Formation

The requirement for oxidized nicotinamide in HSD inactivation and the formation of a highly stable ternary inhibition complex suggested that HON could undergo oxidized $NAD(P)^+$-dependent oxidation to generate a potentially reactive glyoxal derivative (Figure 3, path A); however, inhibition was not affected by the presence of electrophile trapping agents, including glutathione and β-mercaptoethanol, and glyoxal-reactive *D,L*-arginine. Alternatively, a covalent adduct could be formed between C-5 of HON and position C-4 of the nicotinamide ring of NAD^+ (Figure 3, path B). We found evidence for such an adduct in an increase in absorbance in the 320–340 nm region in the inhibited ternary complex and by inactivation of HSD with HON and NAD^+ enriched with ^{13}C at position 4 of the pyridine ring [13]. This resulted in the detection of a signal at 39.39 ppm in the ^{13}C NMR spectrum of the inactivated complex, consistent with a change in C4 hybridization from sp^2 in NAD^+ to sp^3 in the predicted adduct.

Unequivocal evidence for the formation of a covalent adduct between HON and NAD^+ in the active site of HSD was achieved with the crystallization of the inactive complex and the determination of its atomic structure by X-ray diffraction methods (Table 1 and Figure 4A). Continuous electron density is observed between the NAD and HON moieties, which is consistent with formation of an adduct that includes a bond between the C-4 atom of the nicotinamide ring and C-5 of HON (Figure 4B). The NAD moiety of the adduct interacts with HSD in an identical manner to that seen previously in HSD

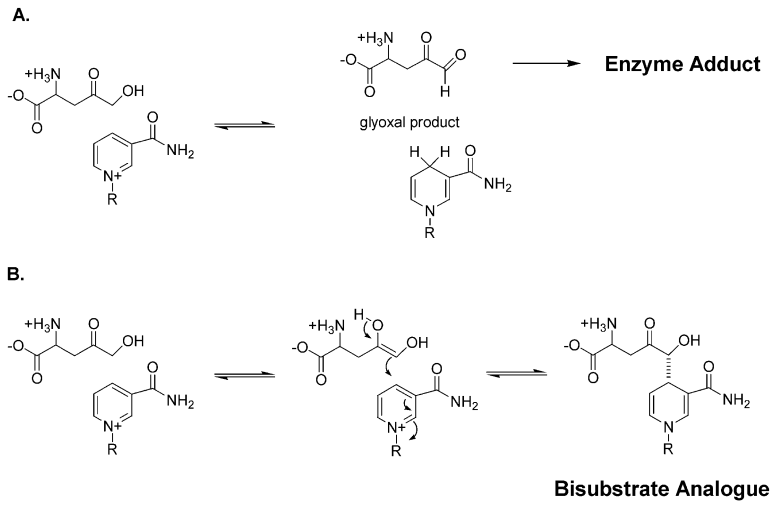

Figure 3. Possible Routes for HSD Inhibition by HON that Require NAD^+

binary and ternary complex structures. The HON moiety of the adduct is, however, positioned and oriented differently than one would expect based on the structure of HSD in complex with Hse (Figure 4C). When comparing HON versus Hse when bound to HSD, HON has rotated ~60°, translated ~1.3 Å, and has altered its C2-C3 torsion angle by ~180°, resulting in an rms distance between common atoms of 3.4 Å. The rotation and translation enables C5 of the HON moiety to be within 1.6 Å of the C4 atom of the nicotinamide ring, thus forming a covalent bond. The altered torsion angle enables the carboxylic acid group of HON to form favorable interactions within the HSD active site, which would otherwise not exist.

Adduct formation results in the creation of a chiral center at the C5 atom of the HON moiety. The electron density for this part of the adduct does not allow us to distinguish between an R or S configuration. Our understanding of the reaction mechanism employed for adduct formation (see below) also does not enable us to definitively predict the chirality of the adduct. Therefore, the current model has both configurations at C5 modeled with equal occupancy.

Table 1. Structural Statistics of the HSD•NAD^+•HON Complex

Data Collection	
Space group	$P4_32_12$
Unit cell (Å)	a = b = 80.9; c = 249.0
Resolution[a] (Å)	2.6 (2.69–2.60)
Completeness (%)	94.6 (72.0)
Reflections (working/test)	24,083/2,356
R_{merge}[b] (%)	8.1 (25.7)
$\langle I/\sigma \rangle$	16.5 (4.0)
Refinement and Model Statistics	
R_{cryst}[c] (%)	23.2
R_{free}[d] (%)	29.5
Rmsd bonds Å	0.007
Rmsd angles (°)	1.4
No. of protein atoms	5420
No. of ligand atoms	55
No. of solvent atoms	40
Average B factor Å	35.1

[a] Number in parentheses refer to highest-resolution shell.
[b] $R_{merge} = \Sigma|I_i - \langle I \rangle|/\Sigma I_i$, where *I* represents the intensities of a multiply measured reflection hkl and $\langle I \rangle$ their average.
[c] $R_{cryst} = \Sigma||F_o| - |F_c||/\Sigma|F_o|$
[d] R_{free} is the crystallographic R factor calculated from 9.8% of the data not included in refinement.

Mechanism of Adduct Formation by HON and Inhibition of HSD

The 3D structure of the HON-inhibited ternary complex provides insight into the mechanism of adduct formation. Formation of the enolate of HON in the active site of HSD bound with NAD^+ sets up the compound for nucleophilic attack of C5 of HON on the nicotinamide ring at C-4 (Figure 5, path A). This would require the assistance of an active site base, though there are no obvious candidates within the vicinity of the predicted deprotonation. A more plausible scenario for adduct formation is that the enol form of HON is the reactive species (Figure 5, path B). For this mechanism Lys223 is required to be neutral, so as to act as a proton acceptor, thus suggesting that the pK value for its primary amine is lower than typical. Given that within a 6 Å radius of the amine the majority of charged groups are positive (Lys117, NAD^+, helix J dipole versus Asp219), a reduction in the pK value for Lys223 is not unexpected. An analogous mechanism that also incorporates a neutral lysine, which acts as a base, has been proposed for NAD-ketone adduct formation in *Drosophila* alcohol dehydrogenase [14].

This pathway accounts for the observed high K_i value, as the enol concentration is expected to be small. Neither we nor previous investigators [15, 16] that have isolated or synthesized HON have detected significant enol content in aqueous solution. To obtain an approximate value for the enol content, we subjected the model compound 1-hydroxy-2-butanone to high-level ab initio minimization and energy calculations (B3LYP/6-3111++G** level) in water using a self-consistent reaction field method based on a Poisson-Boltzmann approach [17–19]. The energy for the expected enediol 1,2-dihydroxybut-1-ene was also calculated under identical conditions. Using this approach, it was determined that the keto form is approximately 13.6

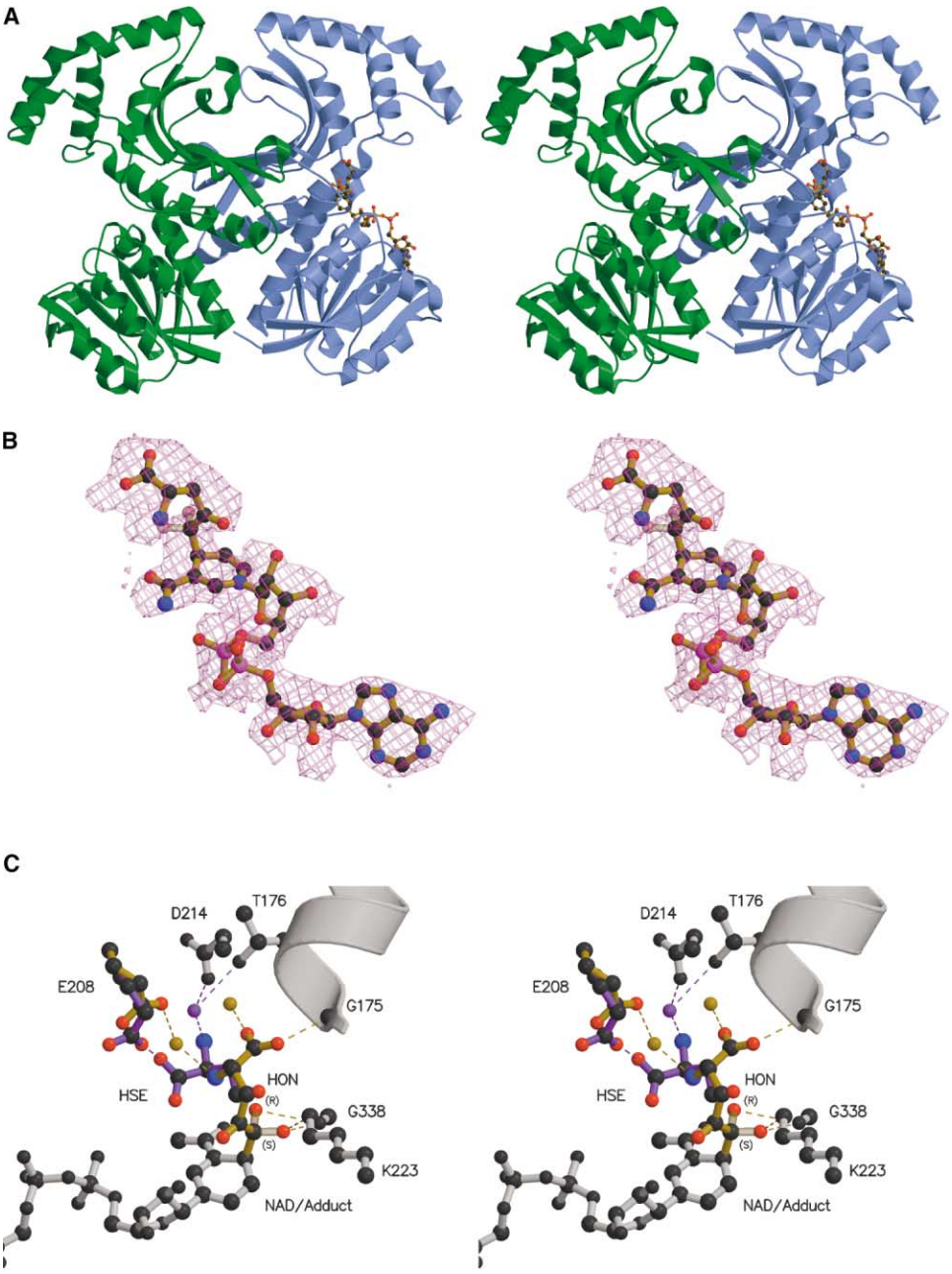

Figure 4. Crystal Structure of HSD with (HON•NAD)-Adduct in the Active Site

(A) Overall fold of the HSD dimer, highlighting the location of the adduct.

(B) $F_o - F_c$ SA-omit map of the (HON•NAD)-adduct contoured at 2σ.

(C) Stereo diagram of the active site of HSD with bound (HON•NAD)-adduct. Also shown in overlay is the structure of HSD with bound NAD analog and HSE. For clarity, for those parts of the structures that do not differ significantly between the two models, only the adduct structure is shown in gray. Residues and side chains with different conformations are colored purple for the HSE-bound structure and gold for the (HON•NAD)-adduct bound structure. Hydrogen bonds are illustrated by dash lines, and the R and S configuration at the C5 atom of the HON moiety are shown using transparencies. Figure was prepared with Molscript [28], Conscript [29], and Raster 3D [30].

kcal/mole more stable than the enediol in water. This corresponds to a predicted 1.1×10^{-8}% enol content for HON in water. This is consistent with values experimentally found for similar types of ketones.

The structure of the HSD•(HON•NAD)-adduct complex also provides a rational explanation for the observed tight binding behavior afforded by the inhibitor, which results in effectively irreversible inhibition. At least two, and possibly three, factors play a role in the high affinity of the adduct for the enzyme. First, because the (HON•NAD)-adduct can be considered a bimolecular mimic of the two substrates, its binding constant is the first approximation of the product of the binding constants for the individual substrates. Second, the HON

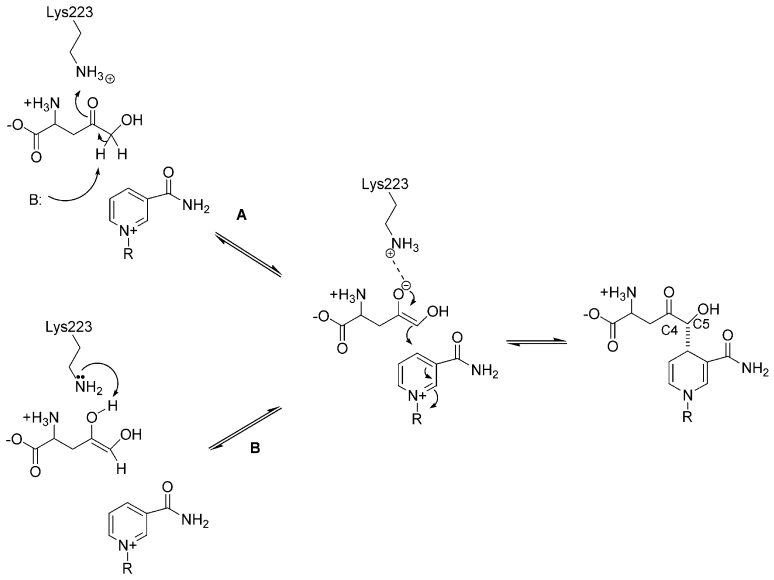

Figure 5. Alternate Mechanisms of Adduct Formation Involving Bond Creation between $NAD(P)^+$ and the HON Enolate or Neutral Enol

Path A, HON enolate; path B, neutral Enol.

moiety forms several strong interactions with HSD (Figure 4C). Specifically, the carboxylate group of HON forms a hydrogen bond with the amide backbone of Gly175. This interaction is further strengthened due to the specific location where it occurs, i.e., Gly175 is positioned at the base of helix J implying that the helix dipole will additionally favorably interact with the negatively charged carboxylic acid group of the HON moiety. Finally, the tight binding behavior can be readily rationalized if the conformation of the (HON•NAD)-adduct closely mimics the transition state for the reaction catalyzed by HSD. However, previous mutagenesis data, geometric considerations for hydride transfer, and the observed differences between Hse and HON when bound to HSD [12] are not fully consistent with the adduct being a true analog of the predicted transition state, though they do not rule it out.

Significance

HON is a promising antimycotic agent that has shown efficacy in both in vitro and in vivo tests against human fungal pathogens [6]. The mechanism of action of HON is through inhibition of HSD. Specifically, HON forms an adduct with the cofactor $NAD(P)^+$ in the active site of HSD. The (HON•NAD(P))-adduct has two unusual and surprising properties. First, it remains effectively irreversibly bound to the HSD active site, making HON an enzyme-assisted suicide inactivator. Second, the (HON•NAD(P))-adduct appears to be unstable outside the context of the HSD active site, because all attempts to isolate the adduct have failed. This detailed dissection of the mechanism of HSD inhibition by HON explains how this antimycotic compound, which displays poor binding affinity in the steady state, is able to arrest fungal growth. While favorable pharmacokinetic properties, such as nontoxicity, are promising, in vivo mouse studies suggest that dosage requirements are prohibitive [6]. The elucidation of the mechanism by which HON confers antifungal properties will enable the development of compounds that target HSD with improved drug-like properties for the treatment of serious fungal infections.

Experimental Procedures

Synthetic Chemistry

HON and 4-oxo-*L*-norvaline were synthesized from the common intermediate (*S*)-3-benzyloxycarbonyl-5-oxo-4-oxazolidineacetic acid [20]. Preparation of the 3-benzyloxycarbonyl-4-(3-diazo-2-oxopropyl)-5-oxazolidinone was accomplished in the same fashion as for the reported glutamate homolog using thionyl chloride followed by reaction with diazomethane [20]. For the synthesis of 4-oxo-norvaline, this diazo compound was reacted with hydrogen iodide in chloroform to produce the protected methyl ketone, which was deprotected to 4-oxo-L-norvaline by either catalytic hydrogenation using ammonium formate and Pd/C in methanol [21, 22] or 30% HBr in acetic acid [23]. For the synthesis of HON, the diazo compound was reacted with glacial acetic acid [24] at 70°C for 2 hr, and purification yielded 3-benzyloxycarbonyl-4-(3-acetoxy-2-oxopropyl)-5-oxazolidinone. Reaction of the acetoxy compound with 30% HBr in acetic acid [23] (23°C for 30 min) to cleave the oxazolidinone followed by hydrolysis of the acetate in 6 N HCl [15] at 23°C for 4 days yielded HON.

$[^{13}C]$-NAD^+ was prepared as previously described [13]. $[^{14}C]$-NAD^+ was purchased from New England Nuclear.

Mass Spectrometry

Positive ion electrospray mass spectrometry of HON-inactivated HSD was performed by at the McMaster Regional Centre for Mass Spectrometry. HSD was denatured with 5% CH_3CN and injected on a Micromass Quattro-LC instrument using CH_3CN/H_2O (1:1) as a solvent.

^{13}C-NMR Spectroscopy

A solution of HSD (15 mg, 0.38 μmol) in TAPS (700 μl) was added to $[^{13}C]$-NAD^+ (0.25 mg, 0.38 μmol) in 1.5 ml microfuge tube. To the solution, 38 μl of 20 mM solution of HON (0.111 mg, 0.75 μmol) was then added, and after mixing, the resulting solution was transferred to a NMR tube. Carbon-13 NMR spectra were recorded on a Bruker Avance DRX-500 spectrometer at 125.771 MHz using a 5 mm broadband inverse probe with triple axis gradient capability. The spectra were acquired over a 28.986 kHz spectral width in 32K data points (0.565 s acquisition time). Spectra that were acquired in 1 hr typically required 3300 scans while the overnight spectrum was acquired in 50,000 scans. The ^{13}C pulse width was 6.0 μs (40° flip angle). A

relaxation delay of 0.5 s was used. The FIDs were processed using exponential multiplication (line broadening, 4.0 Hz) and zero filled to 64K before Fourier transformation.

X-Ray Crystallography

Crystals of the (HON•NAD)-adduct were grown under conditions that were similar to published crystallization conditions for the tetragonal crystal form of HSD [11] with the exception of the addition of five molar excess HON to the protein solution and overnight incubation prior to crystallization. Diffraction data were collected at the X8C beamline of the National Synchrotron Light Source, Brookhaven National Laboratories using a Quantum 4 ADSC CCD detector. Data reduction and scaling were performed with the HKL [25] suite of data processing programs. As a starting model for refinement, the crystal structure of HSD complexed with NAD^+ (excluding solvent molecules; pdb accession 1EBF [12]) was used. Refinement was carried out using CNS [26] and included rigid body, positional, bulk solvent correction, grouped B factor, and restrained individual B factor refinement. Manual model rebuilding was carried out with the program O [27], guided by σ_A-weighted $F_o - F_c$, $2F_o - F_c$, and simulated annealing omit maps. Initial electron density maps revealed that only one of the two available active sites in dimeric HSD was occupied (Figures 4A and 4B), analogous to the structure of HSD with bound NAD^+ [12]. These maps further showed that in addition to a NAD cofactor this active site was occupied by a species that was too large to be solvent and which was located sufficiently close to the nicotinamide ring to suggest covalent linkage. Initially, modeling of free HON was attempted, but this resulted in significant positive peaks in the subsequent $F_o - F_c$ maps, confirming a covalent bond between C5 of HON and C4 of the nicotinamide ring. Two possible adducts were constructed, differing in chirality at the HON C5 position and modeled into the active site. Subsequent electron density maps and monitoring of Rfree did not indicate a convincing preference for either configuration, and thus, the current model describes the chirality of the HON C5 to be 50% S and 50% R (Figure 4C). Individual water molecules were added toward the end of refinement, and these were subject to grouped B factor refinement. Alternate cycles of refinement and manual model rebuilding were continued until no improvement of the free R-factor was observed. Statistics pertaining to both data reduction and model refinement are provided in Table 1.

Acknowledgments

We would like to thank past and present members of the Wright and Berghuis laboratories for their assistance and suggestions. This research was supported by the Natural Sciences and Engineering Research Council of Canada and Crompton Co./Cie. (G.D.W.), and the Canadian Institutes of Health Research (A.M.B.). G.D.W. is supported by a Canada Research Chair in Antibiotic Biochemistry, and A.M.B. is the recipient of a CIHR/Rx&D-HRF Research Career Award in the Health Sciences and holds a Canada Research Chair in Structural Biology. Beam line X8C at the NSLS-Brookhaven National Laboratories, Upton, NY, is in part supported by a grant from the Natural Sciences and Engineering Research Council of Canada and the Canadian Institutes of Health Research.

Received: July 2, 2003
Revised: August 11, 2003
Accepted: August 11, 2003
Published: October 17, 2003

References

1. Sternberg, S. (1994). The emerging fungal threat. Science *266*, 1632–1634.
2. Groll, A.H., and Walsh, T.J. (2001). Uncommon opportunistic fungi: new nosocomial threats. Clin. Microbiol. Infect. *7* (*Suppl 2*), 8–24.
3. Dixon, D.M., McNeil, M.M., Cohen, M.L., Gellin, B.G., and La Montagne, J.R. (1996). Fungal infections: a growing threat. Public Health Rep. *111*, 226–235.
4. Loeffler, J., and Stevens, D.A. (2003). Antifungal drug resistance. Clin. Infect. Dis. *36*, S31–S41.
5. Tatasuoka, S., Miyake, A., Hitomi, H., Ueyanagi, J., Iwasaki, H., Yamaguchi, T., Kanazwa, K.-I., Araki, T., Tsuchiya, K., Hiraiwa, F., et al. (1961). HON, a new antibiotic produced by *Streptomyces akiyoshiensis nov. sp*. J. Antibiot. *14*, 39–43.
6. Yamaguchi, H., Uchida, K., Hiratani, T., Nagate, T., Watanabe, N., and Omura, S. (1988). RI-331, a new antifungal antibiotic. Ann. N Y Acad. Sci. *544*, 188–190.
7. Yamaki, H., Yamaguchi, M., and Yamaguchi, H. (1992). Mechanism of the antifungal action of (S) 2-amino-4-oxo-5-hydroxypentanoic acid, RI-331. In Synthesis and Chemistry of Agrochemicals III, D.R. Baker, J.G. Fenyes, and J.J. Steffens, eds. (Washington, DC: American Chemical Society), pp. 428–442.
8. Yamaki, H., Yamaguchi, M., Suzuki, H., Nishimura, T., Saito, H., and Yamaguchi, H. (1990). The mechanism of antifungal action of (S)-2-amino-4-oxo-5-hydroxypentanoic acid, RI-331: the inhibition of homoserine dehydrogenase in *Saccharomyces cerevisiae*. Biochem. Biophys. Res. Commun. *168*, 837–843.
9. Yamaki, H., Yamaguchi, M., Tsuruo, T., and Yamaguchi, H. (1992). Mechanism of action of an antifungal antibiotic, RI-331, (S) 2-amino-4-oxo-5-hydroxypentanoic acid: kinetics of inactivation of homoserine dehydrogenase from *Saccharomyces cerevisiae*. J. Antibiot. *45*, 750–755.
10. Jacques, S.L., Ejim, L.J., and Wright, G.D. (2001). Homoserine dehydrogenase from *Saccharomyces cerevisiae*: kinetic mechanism and stereochemistry of hydride transfer. Biochim. Biophys. Acta *1544*, 42–54.
11. DeLaBarre, B., Jacques, S.L., Pratt, C.E., Ruth, D.A., Wright, G.D., and Berghuis, A.M. (1998). Crystallization and preliminary X-ray diffraction studies of homoserine dehydrogenase from *Saccharomyces cerevisiae*. Acta Crystallogr. D Biol. Crystallogr. *54*, 413–415.
12. DeLaBarre, B., Thompson, P.R., Wright, G.D., and Berghuis, A.M. (2000). Crystal structures of homoserine dehydrogenase suggest a novel catalytic mechanism for oxidoreductases. Nat. Struct. Biol. *7*, 238–244.
13. Oberfrank, M., Hull, W.E., and Retey, J. (1984). Synthesis and properties of (4-^{13}C)NAD^+. Observation of its binding to yeast alcohol dehydrogenase by ^{13}C-NMR spectroscopy. Eur. J. Biochem. *140*, 157–161.
14. Benach, J., Atrian, S., Gonzalez-Duarte, R., and Ladenstein, R. (1999). The catalytic reaction and inhibition mechanism of Drosophila alcohol dehydrogenase: observation of an enzyme-bound NAD-ketone adduct at 1.4 Å resolution by X-ray crystallography. J. Mol. Biol. *289*, 335–355.
15. Mooiweer, H.H., Ettema, K.W.A., Hiemstra, H., and Speckamp, W.N. (1990). Preparation of γoxo-α-amino acids from silyl enol ethers and glycine cation equivalents; a facile synthesis of (±)-5-hydroxy-4-oxonorvaline (HON). Tetrahedron *46*, 2991–2998.
16. White, R.L., Smith, K.C., and DeMarco, A.C. (1994). Biosynthesis of 5-Hydroxy-4-oxo-L-norvaline in *Streptomyces akiyoshiensis*. Can. J. Chem. *72*, 1645–1655.
17. Schrodinger, L.L.C. (2002). Jaguar 5.0: Portland, OR.
18. Tannor, D.J., Marten, B., Murphy, R., Friesner, R.A., Sitkoff, D., Nicholls, A., Ringnalda, M., III, W.A.G., and Honig, B. (1994). Accurate first principles calculation of molecular charge distributions and solvation energies from Ab initio quantum mechanics and continuum dielectric theory. J. Am. Chem. Soc. *116*, 11875–11882.
19. Marten, B., Kim, K., Cortis, C., Friesner, R.A., Murphy, R.B., Ringnalda, M.N., Sitkoff, D., and Honig, B. (1996). New model for calculation of solvation free energies: correction of self-consistent reaction field continuum dielectric theory for short-range hydrogen-bonding effects. J. Phys. Chem. *100*, 11775–11788.
20. Scholtz, J.A., and Bartlett, P.A. (1989). A convenient differential protection strategy for functional group manipulation of aspartic and glutamic acids. Synthesis, 542–544.
21. Anwer, M.K., and Spatola, A.F. (1980). An advantageous method for rapid removal of hydrogenolysable protecting groups under ambient conditions: synthesis of leucine enkephalin. Synthesis, 929–932.

22. Itoh, M. (1969). Peptides. I. Selective protection of alfa- or side-chain carboxyl groups of aspartic and glutamic acid. A facile synthesis of beta-aspartyl and beta-glutamyl peptides. Chem. Pharm. Bull. *17*, 1679–1686.
23. Ben-Ishai, D., and Berger, A. (1952). Cleavage of N-carbobenzoxy groups by dry hydrogen bromide and hydrogen chloride. J. Org. Chem. *17*, 1564–1570.
24. Chang, P.K., Sciarini, L.J., and Handschumacher, R.E. (1973). New asparagine analogs. J. Med. Chem. *16*, 1277–1280.
25. Otwinowski, Z., and Minor, W. (1997). Processing of X-ray diffraction data collected in oscillation mode. Macromolecular Crystallogr. A *276*, 307–326.
26. Brunger, A.T., Adams, P.D., Clore, G.M., DeLano, W.L., Gros, P., Grosse-Kunstleve, R.W., Jiang, J.S., Kuszewski, J., Nilges, M., Pannu, N.S., et al. (1998). Crystallography & NMR system: a new software suite for macromolecular structure determination. Acta Crystallogr. D Biol. Crystallogr. *54*, 905–921.
27. Jones, T.A., Zou, J.Y., Cowan, S.W., and Kjeldgaard (1991). Improved methods for binding protein models in electron density maps and the location of errors in these models. Acta Crystallogr. A *47*, 110–119.
28. Kraulis, P.J. (1991). MOLSCRIPT: a program to produce both detailed and schematic plots of protein structures. J. Appl. Crystallogr. *24*, 946–950.
29. Lawrence, M.P., and Bourke, P. (2000). CONSCRIPT: a program for generating electron density isosurfaces for presentation in protein crystallography. J. Appl. Crystallogr. *33*, 990–991.
30. Merritt, E.A., and Bacon, D.J. (1997). Raster3D: photorealistic molecular graphics. Macromolecular Crystallogr. B *277*, 505–524.

Accession Numbers

Crystallographic coordinates and structure factor amplitudes have been deposited in the Protein Data Bank (accession code 1Q7G).